Hanada S Takewa Y, Tsukiya T, Mizuno T, Taenaka Y, Tatsumi E	Effect of the technique for assisting renal blood circulation on ischemic kidney in acute cardiorenal syndrome	J Artif Organs	15	140-145	2012
Osa M, Masuzawa T, Tatsumi E	Miniaturized axial gap maglev motor with vector control for pediatric artificial heart	日本AEM学会誌	20	397-403	2012
Ando M, Nishimura T, Takewa Y, Kyo S, Ono M, Taenaka Y, Tatsumi E	Creating an ideal off-test mode for rotary left ventricular assist devices: Establishing a safe and appropriate weaning protocol after myocardial recovery	J Thorac Cardiovasc Surg	143	1176-1182	2012
Takewa Y, Yamanami M, Kishimoto Y, Arakawa M, Kanda K, Matsui Y, Oie T, Ishibshi-Uchida H, Tajikawa T, Ohba K, Yaku H, Taenaka Y, Tatsumi E, Nakayama Y	In vivo evaluation of an in-body, tissue-engineered, completely autologous valved conduit (biovalve type VI) as an aortic valve in a goat model	J Artif Organs		Published on line (DOI: 10.1007/s10047-012-0679-8)	2012
Sawa Y, Tatsumi E, Funakubo A, Horiuchi T, Iwasaki K, Kishida A, Masuzawa T, Matsuda K, Myoui A, Nishimura M, Nishimura T, Tokunaga S, Tomizawa Y, Tomo T, Yamaoka T	Journal of Artificial Organs 2011: the year in review	J Artif Organs	15	11-19	2012
巽　英介	わが国における先進医療機器の研究開発・臨床応用・製品化に関する諸問題と対策	日本機械学会誌	114	9-12	2011
巽　英介	先進医療機器の開発・製品化における現在の課題と取組み	研究開発リーダー	8	21-25	2012
巽　英介	先端医療機器の研究開発・臨床応用・製品化における諸問題	平成23年度東京理科大学総合研究機構インテリジェントシステム研究部門研究成果報告会論文集		1-3	2012

築谷朋典	人工心臓の実用化－人工心臓をつけて家族のもとへ帰ろう－	日本機械学会誌	115	38-39	2012
巽　英介	人工肺と ECMO/PCPS	日本体外循環技術医学会教育セミナーテキスト	28	21-29	2012
巽　英介	抗血栓性と長期耐久性に優れた次世代型人工肺および ECMO/PCPS システムの開発と製品化	医療機器学	82	472-478	2012
巽　英介	先進医療機器の研究開発・臨床応用・製品化における課題	第１回早期・探索的臨床試験拠点 Joint Symposium アカデミア発医療イノベーション －ALL Japan パラダイムシフト－ 講演集		26-37	2012
Umeki A, Nishimura T, Takewa Y, Ando M, Arakawa M, Kishimoto Y, Tsukiya T, Mizuno T, Kyo S, Ono M, Taenaka Y, Tatsumi E	Change in myocardial oxygen consumption employing continuous-flow LVAD with cardiac beat synchronizing system, in acute ischemic heart failure models	J Artif Organs		Published on line (DOI: 10.1007/s10047-012-0682-0)	2013
Kishimoto Y, Takewa Y, Arakawa M, Umeki A, Ando M, Nishimura T, Fujii Y, Mizuno T, Nishimura M, Tatsumi E	Development of a novel drive mode to prevent aortic insufficiency during continuous-flow LVAD support by synchronizing rotational speed with heartbeat	J Artif Organs		Published on line (DOI: 10.1007/s10047-012-0685-x)	2013
Sumikura H, Homma A, Ohnuma K, Taenaka Y, Takewa Y, Mukaibayashi H, Katano K, Tatsumi E	Development and evaluation of endurance test system for ventricular assist devices	J Artif Organs		Published on line (DOI: 10.1007/s10047-013-0687-3)	2013
Tsukiya T, Mizuno T, Takewa Y, Yamane T, Hoshi H, Okubo T, Osada T, Tatsumi E, Taenaka Y	Preclinical evaluation of a cardiopulmonary support system consisting of the newly-developed centrifugal pump with a unique hydrodynamic bearing	20th Congress of the International Society for Rotary Blood Pumps		80	2012

Ando M, Takewa Y Nishimura T, Yamazaki K, KyoS Ono M, Tsukiya T, Mizuno T, Taenaka Y, Tatsumi E	Coronary Vascular Resistance Increases Under Full Bypass Support o F Centrifugal Pumps Relation Between Myocardial Perfusion and Ventricular Workload During Pump Support	Artif Organs		105-110	2012
Nakayama Y	Hyperbranched polymeric "star vectors" for effective DNA or siRNA delivery	Acc Chem Res	45	994-1004	2012
Iwai R, Kusakabe S, Nemoto Y, Nakayama Y	Deposition gene transfection using bioconjugates of DNA and thermo responsive cationic homopolymer	Bioconjug Chem	23	751-757	2012
Moriwaki T, Oie T, Takamizawa K, Murayama Y, Fukuda T, Omata S, Nakayama Y	Observation of local elastic distribution in aortic tissues under static straincondition by use of a scanning haptic microscope	J Artif Organs	16	91-97	2013
Moriwaki T, Oie T, Takamizawa K, Murayama Y, Fukuda T, Omata S, Nakayama Y	Surface density mapping of natural tissue by a scanning haptic microscope (SHM)	J Med Eng Technol	37	96-101	2013
Yamanami M, Ishibashi-Ueda H, Yamamoto A, Iida H, Watanabe T, Kanda K, Yaku H, Nakayama Y	Implantation study of small-caliber "biotube" vascular grafts in a rat model	J Artif Organs	16	59-65	2013
Iwai R, Haruki R, Nemoto Y, Nakayama Y	Enhanced transfection efficiency of poly(N,N-dimethylaminoethyl methacrylate)-based deposition transfection by combination with tris(hydroxymethyl)aminomethane	Bioconjug Chem	24	159-166	2013
Ando H, Ooshima M, Nakayama Y, Nakayama A	Polyethylene Glycol-solvolyzed Poly-(L)-lactic Acids and Their Stereocomplexes with Poly-(D)-lactic Acid	Polymer Degradation and Stability	98	958-962	2013
中山泰秀	体内で作るバイオマテリアル	化学工業	163	35-41	2012

中山泰秀，田地川勉，西正吾	脳動脈瘤治療用の多孔化カバーステント開発における孔設計の重要性	循環器病研究の進歩	33	54-73	2012
山原研一，中山泰秀，寒川賢治	国立循環器病研究センターの再生医療研究の現状に関して	循環器病研究の進歩	33	74-81	2012
Nishikawa Y, Satow T, Takagi T, Murao K, Miyamoto S, Iihara K	Efficacy and Safety of Single versus Dual Antiplatelet Therapy for Coiling of Unruptured Aneurysms	J Stroke Cerebrovasc Dis			In press
Iihara K, Satow T, Matsushige T, Kataoka H, Nakajima N, Fukuda K, Isozaki M, Maruyama D, Nakae T, Hashimoto N	Hybrid Operating Room for the Treatment of Complex Neurovascular and Brachiocephalic Lesions	J Stroke Cerebrovasc Dis			In press
Satow T, Murao K, Matsushige T, Fukuda K, Miyamoto S, Iihara K	Superselective Shunt Occlusion for the Treatment of Cavernous Sinus Dural Arteriovenous Fistulas	Neurosurgery			In press
Ohnishi H, Iihara K, Kaku Y, Yamauchi K, Fukuda K, Nishimura K, Nakai M, Satow T, Nakajima N, Ikegawa M	Haptoglobin Phenotype Predicts Cerebral Vasospasm and clinical Deterioration after Aneurysmal Subarahnoid Hemorrhage	J Stroke Cerebrovasc Dis	22	520-526	2013
田地川勉，中山雄太，紅林芳嘉，西正吾，中山泰秀	脳動脈瘤治療用多孔薄膜カバードステントの開発（薄膜留置による瘤塞栓性能の評価と微細孔形状の最適化）	日本機械学会論文集B編,			Accepted（掲載資料なし）
Nakayama A, Yamano N, Kawasaki N, Nakayama Y	Synthesis and Biodegradation of Poly(2-pyrrolidone-co-e-caprolactone)s	Polymer Degradation and Stability			Accepted（掲載資料なし）

REFERENCES

1. Rebeyka IM, Hanan SA, Borges MR, et al. Rapid cooling contracture of the myocardium. *J Thorac Cardiovasc Surg* 1990; 100:240–9.
2. Shum-Tim D, Tchervenkov CI, Hosseinzadeh T, Chiu RCJ. Contracture of the newborn myocardium after prolonged prearrest cooling. *J Thorac Cardiovasc Surg* 1993;106:643–50.
3. Otani H, Engelman RM, Rousou JA, Breyer RH, Lemeshow S, Das DK. The mechanism of myocardial reperfusion injury in neonates. *Circulation* 1987;76(Suppl. V):V161–V167.
4. Chiu RC-J, Bindon W. Why are newborn hearts vulnerable to global ischemia? *Circulation* 1987;76(Suppl. V):V146–V149.
5. Wittnich C, Peniston C, Ianuzzo D, Abel JG, Salerno TA. Relative vulnerability of neonatal and adult hearts to ischemic injury. *Circulation* 1987;76(Suppl. V):V156–V160.
6. Downing SE, Chen V. Myocardial hibernation in the ischemic neonatal heart. *Circ Res* 1990;66:763–72.
7. Grice WN, Konishi T, Apstein CS. Resistance of neonatal myocardium to injury during normothermic and hypothermic ischemic arrest and reperfusion. *Circulation* 1987;76(Suppl. V):V150–V155.
8. Stowe DF, Fujita S, An J, Paulsen RA, Varadarajan SG, Smart SC. Modulation of myocardial function and $[Ca^{2+}]$ sensitivity by moderate hypothermia in guinea pig isolated hearts. *Am J Physiol Heart Circ Physiol* 1999;277:H2321–2332.
9. O'Brien JD, Howlett SE, Burton HJ, O'Blenes SB, Litz DS, Friesen CLH. Pediatric cardioplegia strategy results in enhanced calcium metabolism and lower serum troponin T. *Ann Thorac Surg* 2009;87:1517–24.

Coronary Vascular Resistance Increases Under Full Bypass Support of Centrifugal Pumps—Relation Between Myocardial Perfusion and Ventricular Workload During Pump Support

*†Masahiko Ando, *Yoshiaki Takewa, †Takashi Nishimura, ‡Kenji Yamazaki, †Shunei Kyo, §Minoru Ono, *Tomonori Tsukiya, *Toshihide Mizuno, *Yoshiyuki Taenaka, and *Eisuke Tatsumi

*Department of Artificial Organs, National Cerebral and Cardiovascular Center Research Institute, Osaka; †Department of Therapeutic Strategy for Heart Failure; §Department of Cardiothoracic Surgery; University of Tokyo; and ‡Department of Cardiovascular Surgery, Tokyo Women's Medical University, Tokyo, Japan

doi:10.1111/j.1525-1594.2011.01298.x

Received September 2010; revised February 2011.

Address correspondence and reprint requests to Dr. Masahiko Ando, Department of Artificial Organs, National Cerebral and Cardiovascular Center Research Institute, 5-7-1 Fujishiro-dai, Suita, Osaka 565-8565, Japan. E-mail: masandoo@hotmail.com

Presented in part at the 2010 ESAO Meeting held September 8–12, 2010 in Skopje. Macedonia.

Abstract: Coronary circulation is closely linked to myocardial oxygen consumption (MVO_2), and previous reports have suggested decreased coronary flow (CoF) under left ventricular assist device support. Decreased CoF itself under support is not unfavorable because the native heart can be well unloaded and myocardial oxygen demand is also decreased. There should be an autoregulatory system that would maintain optimal CoF according to oxygen demand; however, the detailed mechanism is still unclear. The aim of the current study is to evaluate the effect of centrifugal pumps on CoF under varied bypass rates in relation to left ventricle workload. A centrifugal pump, EVAHEART (Sun Medical Technology Research Corporation, Nagano, Japan), was installed in an adult goat ($n = 10$, 61.3 ± 6.5 kg). We set up the following conditions, including Circuit-Clamp (i.e., no pump support), 50% bypass, and 100% bypass. In these settings, CoF, MVO_2, pressure–volume area (PVA), and coronary vascular resistance (CVR) were measured. In 100% bypass, CoF, MVO_2, and PVA were all decreased significantly from clamp. While in 50% bypass, CoF and MVO_2 decreased from clamp, but not PVA. There was a significant 40% increase in CVR in 100% bypass from clamp. This CVR increase in 100% bypass was possibly due to mechanical collapse of coronary vascular bed itself by pump support or increased vascular tone through autoregulatory system. In clinical settings, we should adjust optimal pump speed so as not to cause this vascular collapse. However, to clarify autoregulatory system of the coronary perfusion, further investigation is ongoing in ischemic and heart failure models. **Key Words:** Left ventricular assist device—Myocardial perfusion—Myocardial oxygen demand.

Coronary circulation is closely linked to myocardial oxygen consumption (MVO_2) (1,2), and previous reports have suggested decreased myocardial perfusion under left ventricular assist device (LVAD) support (3–5). Decreased coronary blood flow during LVAD support in itself is not unfavorable because the native heart can be well unloaded with support and myocardial oxygen demand is also decreased (6,7). There should be an autoregulatory system of coronary blood flow that would maintain optimal myocardial perfusion according to its oxygen demand (1,2,8), and the system could eliminate excessive coronary blood flow when the workload of the native heart is decreased. This intricate regulation has been thought for many years to be through sympathetic neuronal control (9) or chemical mediators, such as adenosine, ATP-dependent K+ channels, nitric oxide, prostaglandins, or inhibition of endothelin (10,11); however, its mechanism in detail has been unclear even to date. (2) Theoretically, the chief and direct determinants of coronary blood flow are: heart rate, arterial blood pressure, especially diastole, and coronary vascular resistance (CVR) (1,12). Out of these three factors, CVR is of great importance especially under LVAD support because it can be affected

by coronary vascular tone, intraventricular pressure, and ventricular wall tension (8). Therefore, we have come to survey the changes in coronary perfusion and CVR under LVAD support.

In the present study, we mainly focused on the effect of a centrifugal LVAD on the amount of coronary flow (CoF) in a normal heart model, in both half and full bypass condition. The influence of LVAD support on myocardial perfusion can be of course different among pump types (13,14), bypass rates (4,6,15), and the native heart function (5,16). In order to build up basic theory, we first did the study in a normal heart model. In previous studies in pulsatile pumps, CoF is normally decreased by support in normal heart model (4) and increased in heart failure model (5,14); however, studies in rotary pumps are still limited and the results are different among reports. The one major difference between pump types is that in pulsatile pumps, the native heart can dilate more easily when pumps are ejecting, while in rotary pumps, the native heart relaxation is more difficult because pumps are continuously ejecting through systole and diastole. Another major difference between axial and centrifugal pump is the flow difference in one cardiac cycle. It can vary more in centrifugal LVAD support due to its mechanical feature (17). In other words, in centrifugal pumps, diastolic flow can be decreased when the pressure head (i.e., aortic pressure [AoP]–left ventricular pressure) becomes relatively high, and this feature might affect coronary perfusion. Indeed, Voitl et al. had reported that coronary perfusion did not decrease by axial pump support in a normal heart model (18).

The aim of the current study is to evaluate the effect of centrifugal pumps on coronary circulation under varied bypass rate in relation to left ventricle (LV) workload. Especially, we focused on the changes in CVR and made some medical and physiological suggestions under rotary LVAD support in clinical practice.

MATERIALS AND METHODS

Experiments were performed on 10 adult goats (61.3 ± 6.5 kg). The animals were fixed in the right recumbent position and intubated. Via left thoracotomy, pressure lines for AoP and central venous pressure (CVP) monitoring were established. We placed an 18 mm electromagnetic flow probe (EMF-1000, Nihon Kohden, Tokyo, Japan) for monitoring ascending aortic flow (AoF). An ultrasonic flow probe (HQD3FSB, Transonic System, Inc., Ithaca, NY, USA) was attached for the monitoring of CoF on the main trunk of the left coronary artery. A 16-mm outflow cannula was sutured to the descending aorta, and 16 mm ultrasonic flow probe (TS420, Transonic) was placed for the monitoring pump flow (PF). After systemic heparinization, a 20-mm inflow cannula was inserted into the LV from the apex. Both the outflow and inflow cannulae were connected to the EVA-HEART (Sun Medical Technology Research Corporation, Nagano, Japan) (17), and we started left heart bypass. A 4Fr Mikro-tip catheter pressure transducer (Millar Instruments, Houston, TX, USA) and a 6Fr conductance catheter (2S-RH-6DA-116, 6 mm, Taisho Biomed Instrument Co., Ltd, Osaka, Japan) were inserted from the anterior wall of the LV for the monitoring of pressure–volume loop (PV loop). The inferior vena cava was taped for the preload reduction to obtain end-systolic pressure–volume relationship (ESPVR). All these experimental protocols were approved by the Animal Research Committee of the National Cerebral and Cardiovascular Center Research Institute and conducted according to its guidelines under the care of a veterinarian.

In the present study, we set up the following three conditions: (A) Circuit-Clamp (i.e., no pump support); (B) 50% bypass; and (C) 100% bypass. Bypass rate was calculated by dividing PF by the sum of PF and AoF. Systemic vascular resistance (SVR) was calculated by dividing the difference between AoP and CVP by total flow, which is the sum of PF and AoF. CVR was calculated by dividing that difference by CoF. SVR and CVR were shown in the ratio, regarded the value in (A) clamp as a baseline. After the experiment, we measured the weight of the LV, and CoF was normalized to the amounts per the LV 200 g.

A 10-Fr retrograde cardioplegic catheter (Gandry RCSP catheter, 94110, Medtronic Japan Co., Ltd, Tokyo, Japan) was inserted to the coronary sinus through the left azygos vein. A balloon was inflated and coronary vein blood was drawn from the small hole which was manually made just before the balloon. We calculated MVO_2 using the following formula as previously reported (4,6,7,18).

$$MVO_2\,(O_2\ mL/min) = \{(ScaO_2 - ScvO_2) \times 1.34 \times aHb + (PcaO_2 - PcvO_2) \times 0.003\} \times 0.01 \times CoF\ (mL/min)$$

where $ScaO_2$ ($ScvO_2$) = oxygen saturation of the coronary artery (vein) blood; $PcaO_2$ ($PcvO_2$), mm Hg = partial pressure of the coronary artery (vein) blood; and aHb, g/dL = hemoglobin concentration of the coronary artery blood. In the results, we showed normalized MVO_2 per beat per LV weight of 100 g. We also showed $SatO_2$ gap (i.e.,

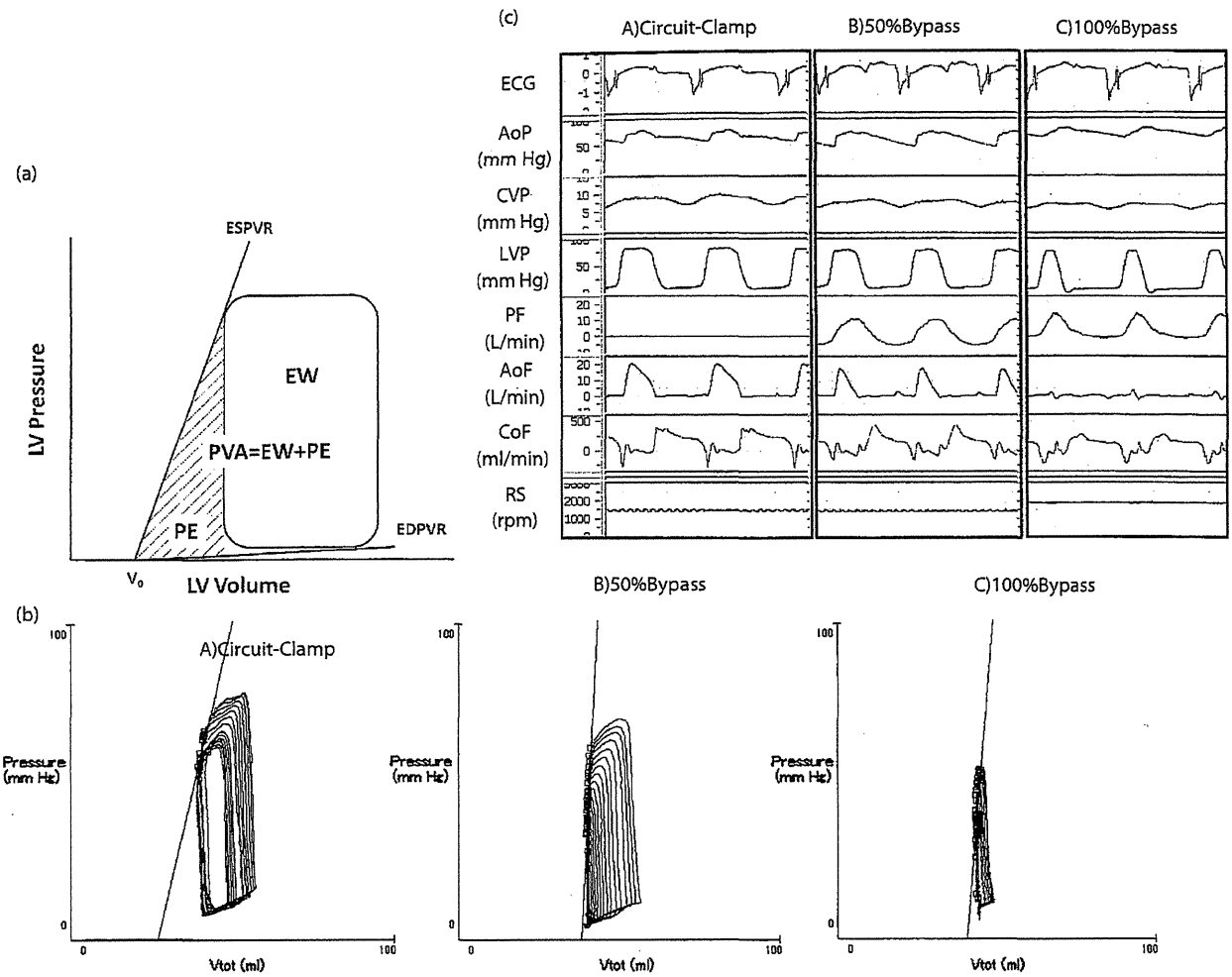

FIG. 1. (a) Schema of pressure–volume loop. PVA is a sum of EW and PE. EW, external work; PE, potential energy; PVA, pressure–volume area; ESPVR, end-systolic pressure–volume relationship; EDPVR, end-diastolic pressure–volume relationship; V_0, *X*-axis intercept of the ESPVR slope. (b) Pressure and flow waveforms. ECG, electrocardiogram; AoP, aortic pressure; CVP, central venous pressure; LVP, left ventricular pressure; PF, pump flow; AoF, ascending aortic flow; CoF, coronary flow; RS, rotational speed. (c) Pressure–volume loops in varied bypass rates. Similar loops were obtained in both (A) and (B) conditions. In (C) conditions, loop size is much smaller than the other two conditions.

$=ScaO_2 - ScvO_2$), which is a main determinant of MVO_2 as well as CoF.

Sigma5 DF system (CD Leycom, Zoetermeer, The Netherlands) was used for the PV loop analysis. The slope of the ESPVR was obtained by gradually occluding the inferior vena cava (7). Pressure–volume area (PVA), which has been recognized as a measure of total mechanical energy and correlates linearly with MVO_2 regardless of changes in loading conditions (19), was approximated by the previously established method (7,19). Briefly, as shown in Fig. 1a, external work (EW) is a computed area in the PV loop, and potential energy (PE) is a crescent area between the ESPVR slope and the straight line of isovolumic relaxation (Fig. 1a). PVA is a sum of EW and PE and is shown in the normalized value per left ventricular weight of 100 g.

The comparison was performed by repeated analysis of variance followed by Tukey's multiple comparison test, and *P* value less than 0.05 was considered as statistically significant.

RESULTS

Figure 1b shows sample waveforms of pressure and flow data. In (B) 50% bypass, when PF and AoF become nearly equal, a small amount of negative PF can be seen in the late diastole, and diastolic AoP

TABLE 1. *Changes in hemodynamic parameters by varied assist rates*

Mode	(A) Clamp	(B) 50% bypass	(C) 100% bypass
Heart rate (rpm)	85.4 ± 8.8	82.1 ± 12.5	80.4 ± 14.4
Mean CVP (mm Hg)	9.8 ± 2.5	9.9 ± 2.4	9.9 ± 2.6
Mean AoP (mm Hg)	66.5 ± 10.7	64.2 ± 9.7	68.2 ± 10.7
Diastolic AoP (mm Hg)	60.5 ± 10.8	58.7 ± 10.0	66.1 ± 10.8
Mean LVP (mm Hg)	46.0 ± 6.5	41.9 ± 8.3	31.1 ± 9.1*†
RS (rpm)	0.0 ± 0.0	1520 ± 162*	2100 ± 149*†
PF (L/min)	0.00 ± 0.00	2.03 ± 0.64*	3.93 ± 1.51*†
AoF (L/min)	4.51 ± 1.30	1.94 ± 0.59*	0.28 ± 0.47*†
Bypass rate (%)	0.0 ± 0.0	51.0 ± 0.6*	93.5 ± 11.1*†
ESP (mm Hg)	81.7 ± 7.9	81.8 ± 14.0	68.7 ± 16.2*†
EDP (mm Hg)	16.0 ± 3.2	15.3 ± 3.3	13.0 ± 3.6*†
ESV (mL)	53.4 ± 10.9	54.3 ± 11.4	53.9 ± 11.7
EDV (mL)	75.3 ± 15.3	75.0 ± 16.4	67.4 ± 15.2*†
Mean CoF (mL/min/LV 200 g)	135.9 ± 29.3	116.7 ± 19.5*	113.5 ± 27.3*
$SatO_2$ gap	0.51 ± 0.10	0.53 ± 0.10	0.41 ± 0.13*†
Hb (g/dL)	9.8 ± 1.7	9.7 ± 1.9	9.6 ± 1.7
MVO_2 (mL/beat/LV 100 g)	0.057 ± 0.012	0.051 ± 0.010*	0.039 ± 0.012*†
PVA (mL × mm Hg/LV100 g)	1246.9 ± 322.3	1276.4 ± 402.0	707.8 ± 380.0*†
EW (mL × mm Hg/LV 100 g)	829.4 ± 248.8	819.4 ± 268.7	402.8 ± 183.9*†
PE (mL × mm Hg/LV 100 g)	417.5 ± 143.2	457.0 ± 254.8	305.6 ± 221.0*†
SVR ratio	1.00 ± 0.0	1.05 ± 0.31	1.15 ± 0.44
CVR ratio	1.00 ± 0.0	1.20 ± 0.37	1.35 ± 0.47*

* means significant change from (A); † means significant change from (B) condition.

CVP, central venous pressure; AoP, aortic pressure; LVP, left ventricular pressure; RS, rotation speed; PF, pump flow; AoF, ascending aortic flow; ESP, end-systolic pressure; EDP, end-diastolic pressure; ESV, end-systolic volume; EDV, end-diastolic volume; CoF, coronary flow; Sat O_2 gap, saturation difference between coronary artery and vein blood; Hb, hemoglobin concentration; MVO_2, myocardial oxygen consumption; PVA, pressure–volume area; EW, external work; PE, potential energy; SVR ratio, systemic vascular resistance ratio regarded (A) as a baseline; CVR ratio, coronary vascular resistance ratio regarded A) as a baseline.

seems to be reduced compared with the other two conditions. In (C) 100% bypass, almost no AoF was observed, and the retrograde flow in diastolic phase was not found at all. As for the waveform of CoF in (A) and (B) conditions, there were flow peaks in the early diastole, while the peak disappeared in (C) 100% bypass, despite the fact that PF in the diastolic phase was well maintained (Fig. 1b).

Table 1 shows all numerical data. There was no significant change in heart rate, mean CVP, mean AoP, or diastolic AoP. In (C) 100% bypass, mean LVP was lower than the other two conditions.

In Fig. 1c, we have shown sample PV loops. In (B) 50% bypass, the loop was similar to that in (A) Clamp, while in (C) 100% bypass, it has become prominently smaller from those in both (A) Clamp and (B) 50% bypass. As shown in Table 1, PVA, EW, and PE were all decreased in (C) 100% bypass, and according to these changes, MVO_2 was also decreased in that condition (Table 1). We have also calculated LV pressure and volume, which revealed that end-systolic pressure, end-diastolic pressure, and end-diastolic volume were significantly decreased in (C) 100% bypass.

CoF was decreased in both (B) 50% and (C) 100% bypass (Table 1), but no difference was observed between these two conditions. In (C) 100% bypass, CVR ratio was significantly increased (Table 1).

DISCUSSION

In the current study, we have investigated left ventricular mechanics and myocardial perfusion during centrifugal LVAD support at varied bypass rates, in relation to the left ventricular workload and MVO_2. In summary, in 50% bypass, LV workload was similar to that in clamp condition; however, CoF was decreased without any change in CVR ratio (Table 1). While in 100% bypass, LV workload was significantly decreased from both clamp and 50% bypass conditions, and CoF was decreased with significant increase in CVR ratio (Table 1).

In fact, few data are available to show the effect of centrifugal LVADs on myocardial perfusion. In the present study, we have measured not only CoF but also MVO_2 and PVA to clarify in detail the relation between these parameters. Our investigation here has made it evident that centrifugal LVADs can reduce CoF in normal heart in both half and full bypass conditions; however, the mechanism of reduced CoF can be different between these two conditions.

In (C) 100% bypass, the PV loop became prominently smaller than that in baseline (Fig. 1c), and PVA and MVO_2 were significantly decreased from both (A) and (B) conditions (Table 1). CoF was also decreased from baseline. As shown previously, MVO_2 is calculated by multiplying $SatO_2$ gap both by Hb and CoF. In the present study, there was no Hb deviation (Table 1); therefore, MVO_2 reduction is mainly due to reduction in CoF and $SatO_2$ gap. During the experiments, $ScaO_2$ was kept at almost 1.0 without exception. So, $SatO_2$ gap reduction actually indicates an increase in $ScvO_2$, which means the LV was effectively decompressed by the full bypass condition, and oxygen demand, or oxygen uptake from the coronary artery blood, was practically decreased.

These changes in the major determinants of MVO_2 during rotary LVAD support are yet to be clearly established even in the current era. Tuzun et al. has reported the decreased MVO_2 and CoF in the normal heart during axial flow LVAD support (4). There were no changes in MVO_2/CoF ratio by varied rotation speed, which indicates that no O_2 gap reduction was present by increasing rotation speed, assuming that there was no Hb deviation. Voitl et al. has suggested that CoF was not decreased by maximal axial pump support; however, MVO_2 was significantly decreased, which implies that MVO_2 reduction was mainly caused by $SatO_2$ gap reduction (18). Contrary to these reports, in the present study, both CoF and $SatO_2$ gap reduction has occurred in full bypass condition. In general, there should be a positive correlation between MVO_2 and CoF (1,2), and $SatO_2$ gap should be decreased under full support condition (1,8). Therefore, our results that both CoF and $SatO_2$ gap were decreased can be acceptable and compatible to the previous reports in physiology (1,2,19).

We have also focused on the changes in CVR, because the amount of CoF can be determined by the following three factors, that is to say, heart rate, AoP, especially diastolic, and CVR (1). In (C) 100% bypass, heart rate is lower than (A) Clamp (Table 1), but the difference was not significant. As for AoP, there was no mean or diastolic AoP deviation between groups. Thus, the key factor could be CVR, and CVR ratio was actually increased in (C) 100% bypass (Table 1). The reason why we obtained increased CVR in (C) 100% bypass is unknown, but we speculate that there should be an autoregulatory system of the coronary artery that might have eliminated the excessive oxygen supply under well-unloaded condition (2,8). There have been many researches on the chemical mediators related to regulation of myocardial perfusion; however, most of these studies focused on the vasodilative effect on the coronary vessels during exercise compared with resting condition (8,10,11,20–22), and the vasoconstrictive effect of these mediators during LVAD support compared with no support condition has yet to be investigated. More research is needed to clarify the autoregulatory mechanism of the coronary artery during LVAD support.

Another reason for the increased CVR in the full bypass condition could be due to the mechanical features of the rotary pump. In pulsatile pumps, there must be a pump systolic phase, and at least during this phase, the native heart can dilate because the mechanical valve between pump chamber and the native heart closes and no vacuum pressure can prevent the native heart from dilation. Whereas in the rotary pump, the situation is different. Rotary LVADs can continuously work through in one cardiac cycle, and especially in full bypass condition, it might affect dilation of the native heart. In diastolic dysfunction without coronary vessel disease, endocardial blood flow is known to be decreased possibly due to collapse of the coronary vascular bed (23). If rotary LVADs had prevented the native heart from dilation in the current study, in the worst case, it might have collapsed the coronary vascular bed, increased CVR, and decreased myocardial perfusion. In order to prevent these vascular bed collapses, we should adjust optimal pump rotational speed so as not to disturb myocardial dilation.

In (B) 50% bypass, a similar PV loop was obtained as in (A) Clamp (Fig. 1c). There were no obvious changes in PVA and pressure data (Table 1); however, a small amount of retrograde PF was observed (Fig. 1a). This retrograde flow was mainly seen in the diastolic phase, when the pressure head (i.e., AoP–LVP) becomes relatively high. Because of this reverse flow, we should definitely recognize that "Half Bypass" is quite different from "Half Support" in left heart bypass with rotary pumps, even if PF is half of the total flow. This reverse flow in half bypass condition was not always present and might have affected the results of the present study. The reason why we did not obtain significant decrease in PVA in (B) 50% bypass despite pump support was possibly due to this reverse flow, and the decrease in CoF in (B) 50% bypass might be caused by this retrograde PF (Table 1).

The present study was performed on normal hearts, and the study on ischemic hearts might have provided different results (5,14–16). Nevertheless, we believe that the current study is considered of value in that we have focused on CVR under rotary LVAD support.

CONCLUSION

CVR increases under full bypass support of centrifugal pumps. In clinical settings, we should adjust pump rotational speed at optimal settings so as not to cause coronary vascular bed collapse. As a physiological rationale, there should be an autoregulatory system of the coronary system, and further investigation is ongoing in ischemic and heart failure models.

REFERENCES

1. Feigl EO. Coronary physiology. *Physiol Rev* 1983;63:1–205.
2. Tune JD, Gorman MW, Feigl EO. Matching coronary blood flow to myocardial oxygen consumption. *J Appl Physiol* 2004;97:404–15.
3. Ootaki Y, Kamohara K, Akiyama M, et al. Phasic coronary blood flow pattern during a continuous flow left ventricular assist support. *Eur J Cardiothorac Surg* 2005;28:711–6.
4. Tuzun E, Eya K, Chee HK, et al. Myocardial hemodynamics, physiology, and perfusion with an axial flow left ventricular assist device in the calf. *ASAIO J* 2004;50:47–53.
5. Noda H, Takano H, Taenaka Y, et al. Regulation of coronary circulation during left ventricular assist. *ASAIO Trans* 1989;35:445–7.
6. Pennock JL, Pierce WS, Prophet GA, Waldhausen JA. Myocardial oxygen utilization during left heart bypass; effect of varying percentage of bypass flow rate. *Arch Surg* 1974; 109:635–41.
7. Kawaguchi O, Sapirstein JS, Daily WB, Pae WE, Pierce WS. Left ventricular mechanics during synchronous left atrial-aortic bypass. *J Thorac Cardiovasc Surg* 1994;107:1503–11.
8. Duncker DJ, Bache RJ. Regulation of coronary blood flow during exercise. *Physiol Rev* 2008;88:1009–86.
9. Haws CW, Green LS, Burgess MJ, Abildskov JA. Effects of cardiac sympathetic nerve stimulation on regional coronary blood flow. *Am J Physiol* 1987;252:H269–74.
10. Duncker DJ, van Zon NS, Ishibashi Y, Bache RJ. Role of k+ atp channels and adenosine in the regulation of coronary blood flow during exercise with normal and restricted coronary blood flow. *J Clin Invest* 1996;97:996–1009.
11. Farias M 3rd, Gorman MW, Savage MV, Feigl EO. Plasma atp during exercise: possible role in regulation of coronary blood flow. *Am J Physiol Heart Circ Physiol* 2005;288:H1586–1590.
12. Klocke FJ, Ellis AK, Orlick AE. Sympathetic influences on coronary perfusion and evolving concepts of driving pressure, resistance, and transmural flow regulation. *Anesthesiology* 1980;52:1–5.
13. Bartoli CR, Giridharan GA, Litwak KN, et al. Hemodynamic responses to continuous versus pulsatile mechanical unloading of the failing left ventricle. *ASAIO J* 2010;56:410–6.
14. Nakata K, Shiono M, Orime Y, et al. Effect of pulsatile and nonpulsatile assist on heart and kidney microcirculation with cardiogenic shock. *Artif Organs* 1996;20:681–4.
15. Nakamura T, Hayashi K, Seki J, et al. Effect of drive mode of left ventricular assist device on the left ventricular mechanics. *Artif Organs* 1988;12:56–66.
16. Hata M, Shiono M, Orime Y, et al. Coronary microcirculation during left heart bypass with a centrifugal pump. *Artif Organs* 1996;20:678–80.
17. Yamazaki K, Saito S, Kihara S, Tagusari O, Kurosawa H. Completely pulsatile high flow circulatory support with a constant-speed centrifugal blood pump: mechanisms and early clinical observations. *Gen Thorac Cardiovasc Surg* 2007;55:158–62.
18. Voitl P, Vollkron M, Bergmeister H, Wieselthaler G, Schima H. Coronary hemodynamics and myocardial oxygen consumption during support with rotary blood pumps. *Artif Organs* 2009;33:77–80.
19. Suga H, Hisano R, Hirata S, Hayashi T, Ninomiya I. Mechanism of higher oxygen consumption rate: pressure-loaded vs. Volume-loaded heart. *Am J Physiol* 1982;242:H942–8.
20. Altman JD, Kinn J, Duncker DJ, Bache RJ. Effect of inhibition of nitric oxide formation on coronary blood flow during exercise in the dog. *Cardiovasc Res* 1994;28:119–24.
21. Gorman MW, Rooke GA, Savage MV, Jayasekara MP, Jacobson KA, Feigl EO. Adenine nucleotide control of coronary blood flow during exercise. *Am J Physiol Heart Circ Physiol* 2010;299:H1981–9.
22. Tune JD, Richmond KN, Gorman MW, Feigl EO. Control of coronary blood flow during exercise. *Exp Biol Med (Maywood)* 2002;227:238–50.
23. Elhabyan AK, Reyes BJ, Hallak O, et al. Subendocardial ischemia without coronary artery disease: is elevated left ventricular end diastolic pressure the culprit? *Curr Med Res Opin* 2004;20:773–7.

Experimental Research With Synthetic Copolymer-Coated Cardiopulmonary Bypass Circuits: Inflammatory and Thrombogenicity Analysis

**Edmo Atique Gabriel,*
**Fredy Max Ayala Montevilla,*
**Valeria Vieira Chida, †Fabio Nunes Dias,*
†Cynara Viterbo Montoya, †Hiroaki Otsubo,
†Zenício Francisco Pires,
and †Sergio Luiz Nogaroto
**Albert Einstein Jewish Hospital, Experimental Surgery Center, São Paulo, Brazil; and †Nipro Medical Brazil, São Paulo, Brazil*

Abstract: This study aimed to assess complement system activation and index of thrombogenicity and platelet aggregation between synthetic copolymer-coated cardiopulmonary bypass (CPB) circuit and conventional CPB circuit. Twenty-six pigs were equally divided into two groups—the conventional group and the coated group. They were placed on CPB for 90 min, and blood samples were collected at three different time points (T0, right before CPB establishment; T1, 45 min after starting CPB; and T2, 90 min after starting CPB) to measure total count of inflammatory cells (leukocytes, neutrophils, lymphocytes, and platelets) and serum levels of fraction C3 of complement system. Upon completion of the 90-min CPB, fragments of different compartments of the CPB circuit were taken for assessing index of thrombogenicity and platelet aggregation. There were no differences between both groups regarding total count of leukocytes, neutrophils, and lymphocytes; however, there was a lower count of platelets at T2 in the coated group ($P = 0.020$). The serum level of fraction C3 was lower in the coated group

doi:10.1111/j.1525-1594.2011.01291.x

Received January 2011; revised March 2011.

Address correspondence and reprint requests to Dr. Edmo Atique Gabriel, Rua Melo Alves, 685, apt # 171, Cerqueira Cesar—01417010, São Paulo, Brazil. E-mail: edag@uol.com.br

J Artif Organs (2012) 15:119–127
DOI 10.1007/s10047-011-0614-4

ORIGINAL ARTICLE

Flow visualization for different port angles of a pulsatile ventricular assist device

Eiki Akagawa · Hwansung Lee · Eisuke Tatsumi · Akihiko Homma · Tomonori Tsukiya · Yoshiyuki Taenaka

Received: 7 August 2008 / Accepted: 10 October 2011 / Published online: 30 October 2011

Abstract The "washout effect" inside a blood pump may depend in part on the configuration of the blood pump, including its "port angle." The port angle, which is primarily decided based on anatomical considerations, may also be important from the rheological viewpoint. In our department, a next-generation diaphragm-type blood pump is being developed. In this study, we examined the influence of the port angle on flow conditions inside our new blood pump. Acrylic resin mock pumps with three different port angles (0°, 30°, and 45°) were prepared for flow visualization. Mechanical monoleaflet valves were mounted on the inlet and outlet ports of the mock pumps. Flow conditions within the mock pumps were visualized by means of particle image velocimetry during a half stroke. As a result, a high flow velocity region was seen along the main circular flow from the inlet to the outlet port. This circular flow was almost uniform and parallel to the plane of the diaphragm-housing junction (DhJ) when viewed from the inlet and outlet sides. Moreover, the proportion of high flow velocity vectors in the plane in the vicinity of the DhJ decreased as the degree of the port angle increased. In conclusion, we found that the flow behavior in the plane in the vicinity of the DhJ changed with the port angle, and that a port angle of 0° may be suitable for our diaphragm-type blood pump in view of the washout effect.

Keywords Pulsatile blood pump · Particle image velocimetry · Port angle · Flow pattern · Washout effect

E. Akagawa (✉) · H. Lee · E. Tatsumi · A. Homma · T. Tsukiya · Y. Taenaka
Department of Artificial Organs, Research Institute, National Cerebral and Cardiovascular Center, 5-7-1 Fujishiro-dai, Suita, Osaka 565-8565, Japan
e-mail: akagawa@ri.ncvc.go.jp

Introduction

One of the most crucial problems when a blood pump is being used is thrombus formation. To prevent this, the "washout effect" has been investigated through the development of different blood pumps [1, 2]. The washout effect depends on the flow behavior inside the blood pump [3, 4]. In the case of a pulsatile blood pump, the flow behavior may be influenced by the design of the artificial valves and the internal configuration of the blood pump. Meanwhile, a next-generation pneumatic ventricular assist device (VAD) is being developed at the National Cerebral and Cardiovascular Center (NCVC) in Japan. The new VAD consists of a diaphragm-type blood pump, intended to improve the washout effect, and a pneumatic compression system. The dimensions of the blood pump (stroke volume 75 mL) are as follows: housing diameter 88 mm, housing thickness 49 mm, and port lumen diameter 19.5 mm. The blood pump is mounted with mechanical monoleaflet valves to commutate the flow direction.

With regard to the design of the artificial valves, the flow of blood passing over the surface of the tilting disk may influence flow conditions inside the blood pump, and the circular flow inside the blood pump may effectively wash the thrombi out from around the diaphragm-housing junction (DhJ). We reported that the orifice direction of the inlet valve exerted a significant influence on the regional flow velocity inside our blood pump [5]. As for the inside configuration of the blood pump, our new blood pump can be employed in various ways as an extracorporeal VAD or an implantable VAD. Therefore, when used as an extracorporeal VAD and the position of the skin cuffs is taken into consideration, the inlet and outlet ports should protrude from the housing parallel to each other (Fig. 1a). When used as an implantable VAD, and the arrangement of the internal

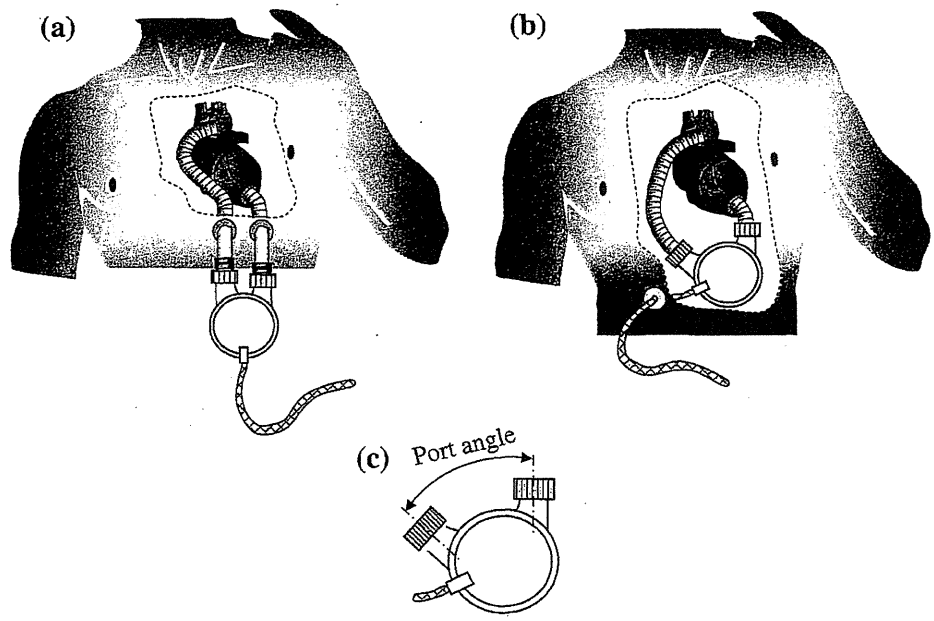

Fig. 1 Description of the next-generation pneumatic VAD. **a** Image of the extracorporeal VAD, **b** image of the implantable VAD, **c** definition of the port angle

organs is taken into consideration, the inlet and outlet ports should protrude from the housing at an acute angle (Fig. 1b). As the washout effect inside the blood pump may depend in part on the configuration of the blood pump, the "port angle" (Fig. 1c), which is usually decided based on anatomical considerations, may be rheologically important.

In a previous study analyzing spatial flow inside a pulsatile blood pump, flow visualization of cross-sections parallel to the circular flow was performed using a diaphragm-type blood pump with a pusher plate mechanism [6]. Although this was a significant study which indicated that the penetration of the inlet jet inside the blood pump was affected by valve orientation, the velocity component of the plane perpendicular to the circular flow was not analyzed. On the other hand, we reported that the orifice direction of the inlet valve exerted a significant influence on the circular flow in the diaphragm-type blood pump we are developing [5]. However, our report evaluated the flow behavior in the plane of circular flow (flow behavior in the plane in the vicinity of the DhJ) from the single direction (front view); the flow behavior in the plane perpendicular to circular flow [flow behavior in the plane of the inlet axis (PIA) and the plane of the outlet axis (POA); perpendicular to the DhJ] was not clarified. The objective of the study described in this report was to evaluate the flow behavior inside our diaphragm-type blood pump using different port angles by flow visualization.

Materials and methods

Flow visualization methods have been used to analyze flow behavior in various flow fields, such as inside blood pumps [4–10] and ventricular models [11, 12]. Three mock pumps made of transparent acrylic resin with different port angles (0°, 30°, and 45°) were prepared for detailed flow visualization (Fig. 2a), and the inside flow was visualized using particle image velocimetry (PIV; Fig. 3). The inside configurations of these pumps were almost the same as that of the blood pump we are developing, with an asymmetric configuration within the housing between the inlet and outlet ports (Fig. 2b). Two mechanical monoleaflet valves (23 mm; Medtronic-Hall™, Medtronic, Minneapolis, MN, USA) were mounted on the inlet and outlet ports of the mock pump. The diaphragm in the mock pump was driven by a control-drive console for the VAD (VCT-30, Toyobo, Osaka, Japan). The mock pump was connected to a Donovan mock circulatory loop tester [13] with vinyl chloride tubes. A diluted suspension (50% glycerin by volume in distilled water, 3.4 cP, 37°C) of polystyrene tracer particles (50 μm, 1.06 g/cm^3) was perfused into the mock circuit. The mean pressure of the chamber connected to the blood pump inflow was maintained in the range from 10 to 20 mmHg, and that connected to the blood pump outflow was kept at approximately 100 mmHg. The pressure waveforms of the inlet, outlet, and driving ports were monitored continuously and recorded using a digital storage unit (PowerLab/16 s, ADInstruments, Nagoya, Japan) by way of a pressure transducer. The outlet flow rate was measured continuously using an ultrasound flowmeter (T106, Transonic Systems, Ithaca, NY, USA).

The three planes of the region measured in the mock pump were illuminated with a light sheet from an argon-ion laser at 488 nm (GLG3680, NEC, Tokyo, Japan). One of the measurement planes (PVDhJ, plane in the vicinity of

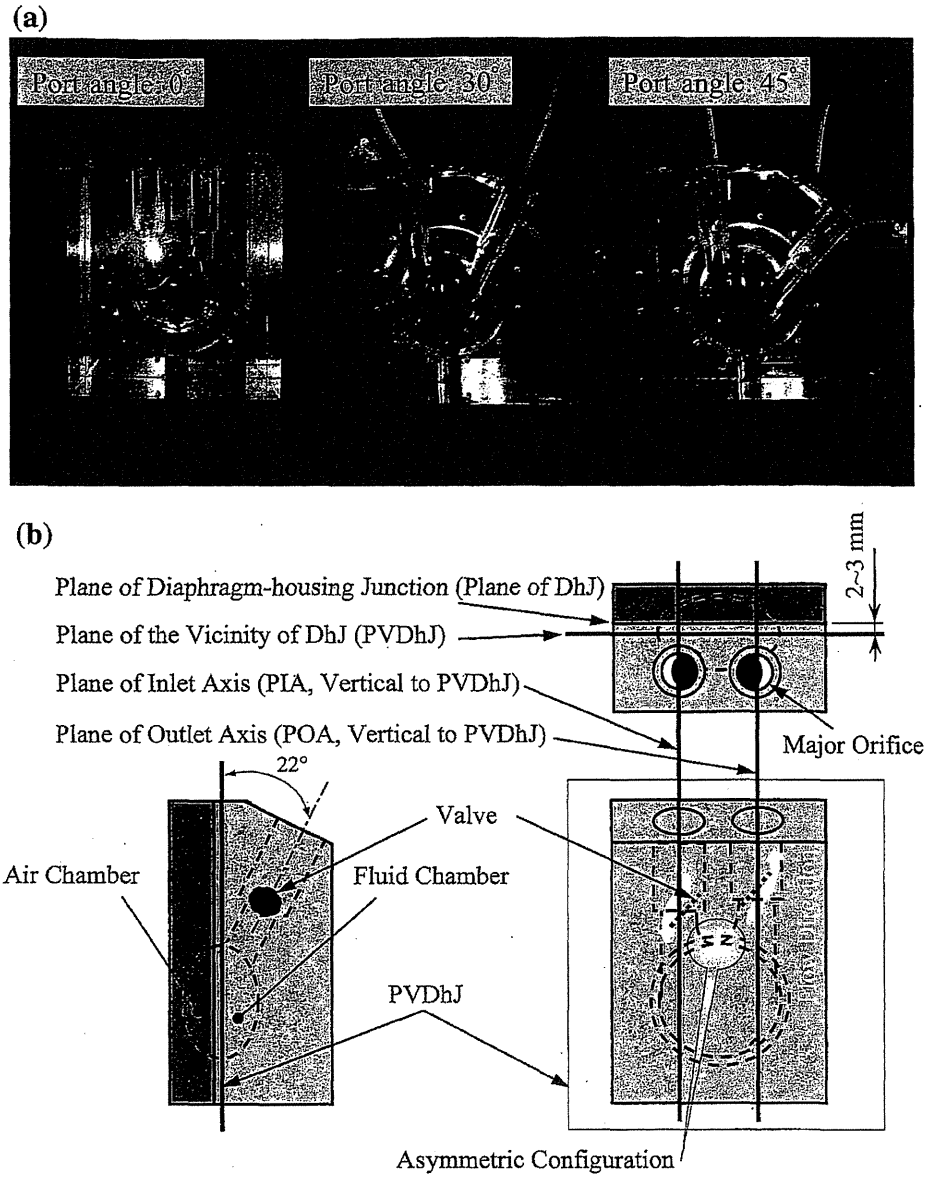

Fig. 2 Configuration of the mock pump. **a** Three mock pumps made of acrylic resin, **b** arrangement of the laser sheet positions. The configuration from the inlet port into the housing was radically expanded, while that from within the housing to the outlet port was moderately narrowed

the DhJ) was parallel to the plane of the DhJ (Fig. 2b; 2–3 mm apart from the plane of the DhJ). The other planes were perpendicular to the PVDhJ and situated on the axes of the inlet and outlet ports (PIA, POA; Fig. 2b). We measured the flow behavior by changing the arrangement of the laser sheet position and the mock pump position (PVDhJ, PIA, and POA at a port angle of 0°; PVDhJ at a port angle of 30°; PVDhJ at a port angle of 45°). The orifice directions of the inlet and outlet valves were set as shown in Fig. 2b. The images of the flow behavior within the blood pump were captured using a high-speed camera (MEMRECAM fx-6000, NAC Image Technology, Tokyo, Japan) operating at 1,000 frames per second. Because the inlet and outlet ports made an angle of 22° with the plane of the DhJ (Fig. 2b), it was also possible to confirm the opening and closing states of the inlet and outlet valves using the recorded images of the front view (same direction associated with the measurement of the flow behavior in the PVDhJ). The image recording was triggered by the falling phase of the function generator waveform (Fig. 4, white arrow, 1.17 Hz). The control-driving console was synchronized with the rising phase of the function generator waveform at a pump rate of 70 beats per minute (systolic duration 35%, positive pressure +230 mmHg, negative pressure −50 mmHg). The movements of tracer particles were registered using the PIV software (Insight 3, TSI Incorporated, MN, Shoreview, USA). The analysis was performed using two frame cross-correlation algorithms

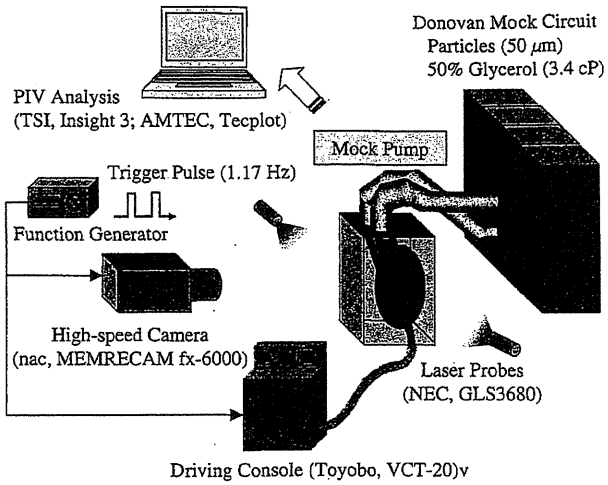

Fig. 3 Flow visualization and mock circulatory system

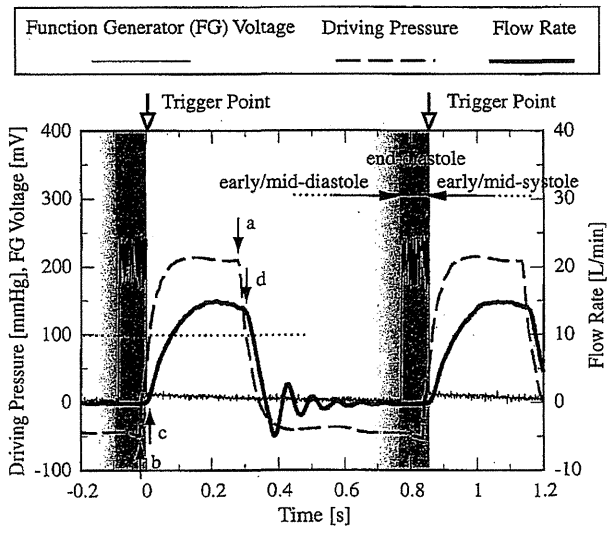

Fig. 4 Waveforms of the driving pressure, the function generator, and the flow rate

and a fast Fourier transform. Flow behavior was quantitated using visualization software for vector mapping (Tecplot 9.2, Tecplot Inc., Bellevue, WA, USA).

Results

The driving console created 4.5 L/min of mock pump output. We measured the flow behavior synchronously with the driving condition, but not simultaneously. The driving pressure waveform, function generator waveform, and outlet flow rate under typical conditions for a port angle of 0° are shown in Fig. 4. We defined partial filling duration as "early/mid-diastole," partial ejection duration as "early/mid-systole," and full filling duration as "end diastole." The diaphragm was moving at early/mid-diastole and early/mid-systole, but it stopped moving at end diastole. The condition of the full-fill/full-eject drive was confirmed by the rectangular-edged configuration of the driving pressure waveform (Fig. 4, arrows a, b). When the driving pressure exceeded the value of 100 mmHg, which was equal to the mean pressure of the chamber connected to the blood pump outflow, the diaphragm started to eject and the flow rate greatly increased (Fig. 4, arrow c). When the driving pressure fell below the value of 100 mmHg, the diaphragm started to fill and the flow rate decreased considerably (Fig. 4, arrow d).

The images of the fluid dynamics in the mock pump analyzed by the PIV method revealed circular flow with flow velocity vectors. Error vectors caused by optical distortion were excluded. The flow patterns at a port angle of 0° in the three planes of the light sheet (PVDhJ, front view; PIA, inlet side view; POA, outlet side view) during a half stroke (0.6–0.9 s after the trigger) are shown in Fig. 5. A high flow velocity region was shown along the main circular flow from the inlet to the outlet port (Fig. 5b–d, front view). This circular flow was almost uniform and parallel to the plane of the DhJ when viewed from the inlet and outlet sides (Fig. 5c, inlet side view and outlet side view). Although the flow velocity inside the inlet port during the diastolic phase suddenly decreased, that inside the outlet port during the systolic phase slowly increased (Fig. 5a, circle A; d, circle B). A flow stagnation region existed in the area between the inlet and outlet port roots in the PVDhJ at mid-diastole and early systole (Fig. 5a, b, d, front view). However, the flow stagnation in this region dissipated and the flow velocity along the circular flow inside the housing was high at end diastole (Fig. 5c, front view). The flow patterns in the PVDhJ during a half stroke for the different port angles are shown in Fig. 6 (average flow velocity at a port angle of 0° <0.19 m/s, that at 30° <0.18 m/s, that at 45° <0.17 m/s; 0.6–0.9 s after the trigger). The orange crosses indicate the center of the circular flow, while the white crosses indicate the trajectories of those centers (Fig. 6). The center of the circular flow was determined manually by viewing the distribution of the flow velocity vectors. The circular flow was orderly and concentric at a port angle of 0°, disorderly at port angles of 30° and 45° (Fig. 6), and eccentric at a port angle of 45°. To evaluate the eccentricity, the trajectory length of the center of the circular flows was measured, as shown in Fig. 7. The trajectory length increased as the port angle increased. At a port angle of 30°, flow distortion occurred downstream of the inlet port during the diastolic phase (Fig. 6, circle A). At a port angle of 45°, flow distortion also occurred downstream of the inlet port during the diastolic phase (Fig. 6, circle B). The frequency distributions of the

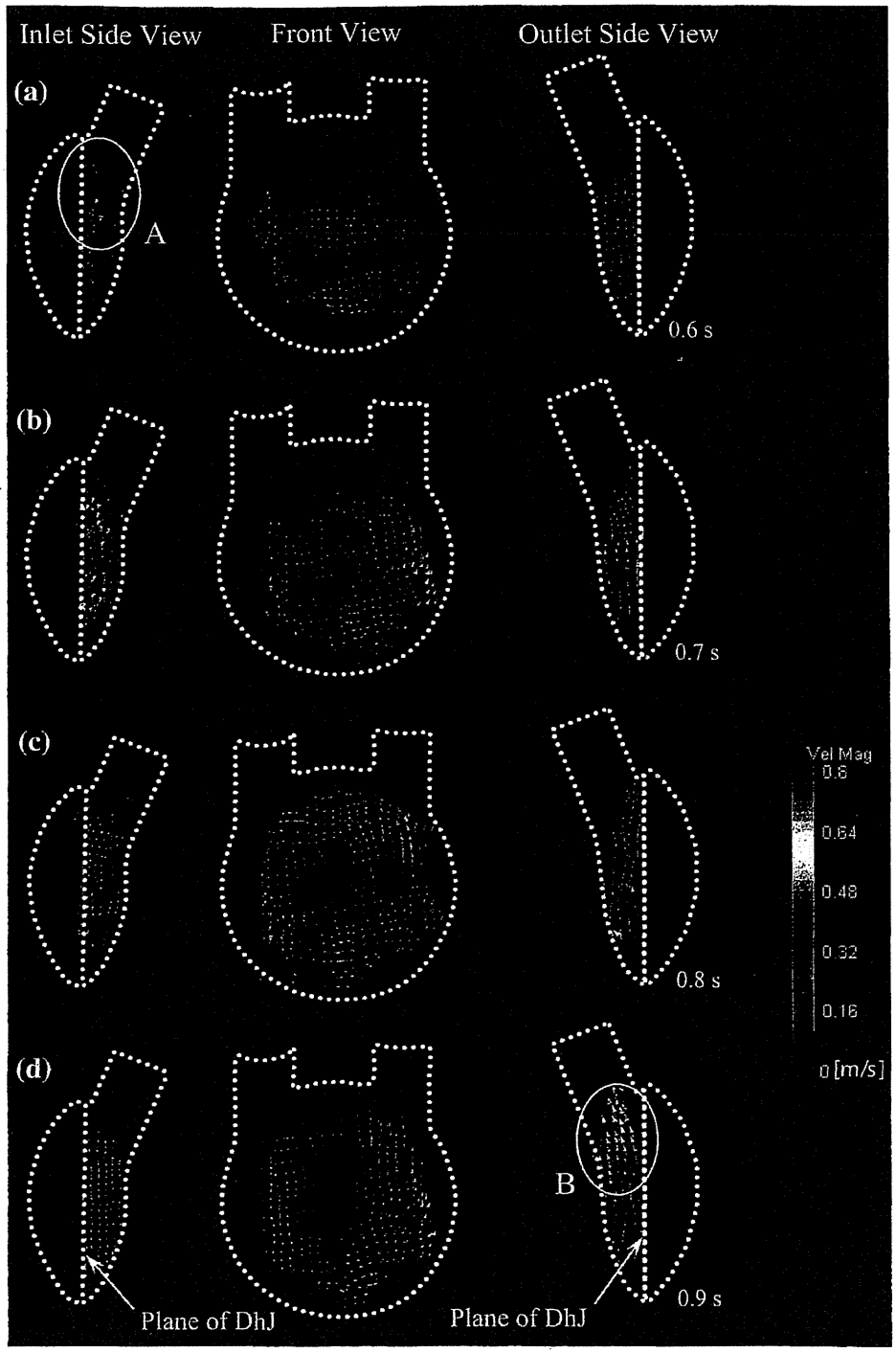

Fig. 5 Flow patterns from three viewpoints during half stroke at a port angle of 0°. **a** 0.6 s after the trigger, **b** 0.7 s after the trigger, **c** 0.8 s after the trigger, **d** 0.9 s after the trigger

magnitude of the flow velocity vectors during end diastole (Fig. 6c, 0.6 s after the trigger) in the PVDhJ are shown in Fig. 8. The proportion of high flow velocity vectors decreased as the port angle increased.

Time-course changes for the opening and closing states of the inlet and outlet valves are shown in Fig. 9a. To evaluate the effects of the port angle on valve motion, the movement durations of the inlet and outlet valves were measured for each port angle, as shown in Fig. 9b. The duration of the completely open state increased and that of the completely closed state shortened as the port angle increased. Although the outlet valve started to open after the inlet valve had almost completely closed at a port angle of 0°, the outlet valve started to open while the inlet valve was still closing at a port angle of 30° (Fig. 9a, 0° and 30°). At a port angle of 45°, the outlet valve started to open

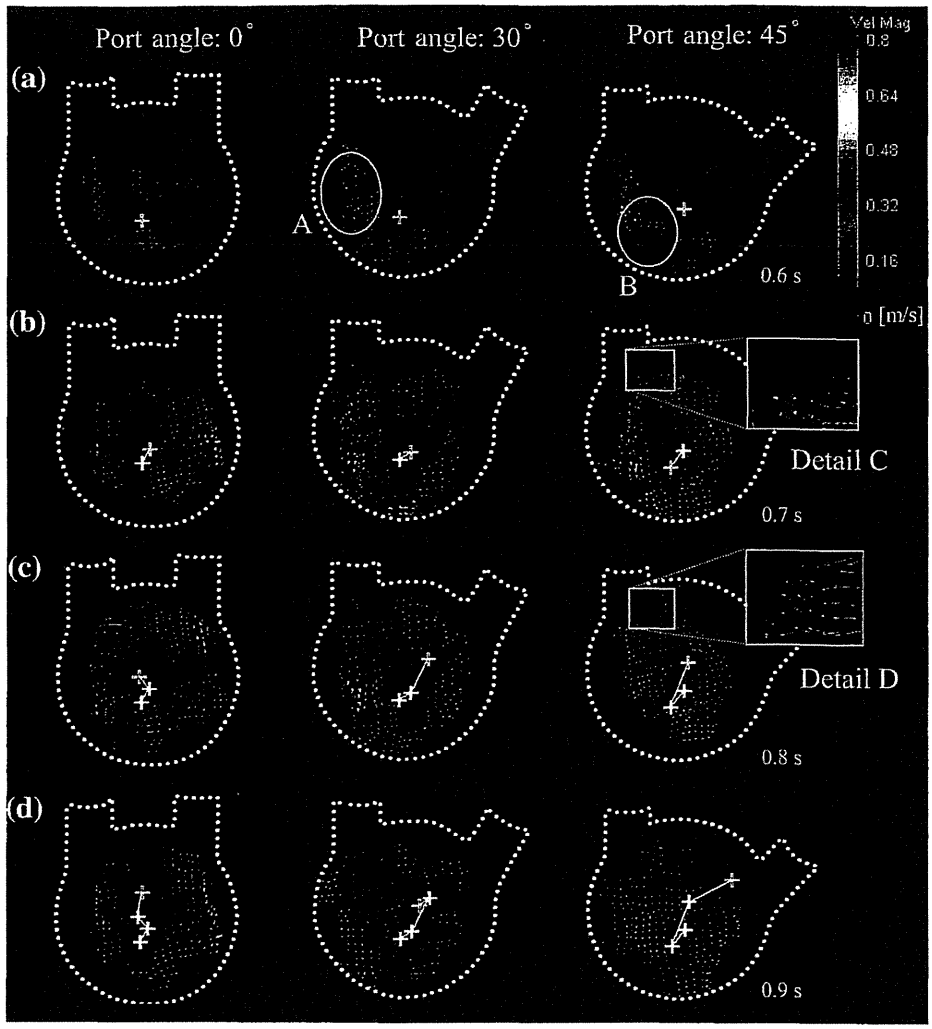

Fig. 6 Flow patterns from the front view during half stroke at port angles of 0°–45°. **a** 0.6 s after the trigger, **b** 0.7 s after the trigger, **c** 0.8 s after the trigger, **d** 0.9 s after the trigger

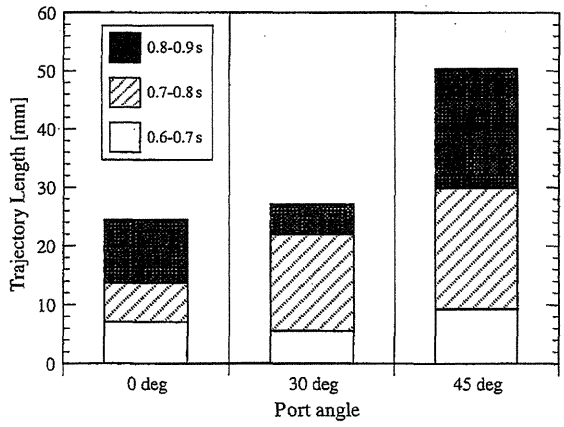

Fig. 7 Trajectory length of the center of the circular flow at port angles of 0–45°

shortly after the inlet valve had started to close (Fig. 9a, 45°). The period of time that both inlet and outlet valves were completely open increased as the port angle increased (Fig. 9b). Although the drive conditions of these port angles were the same, the interval between the points at which the inlet valve started to close and the outlet valve started to open decreased with increasing port angle. Moreover, at the port angle of 45°, a backward flow was seen near the inlet port at mid-diastole to end diastole (Fig. 6, detail C, detail D). Although the inlet valve was open and the inlet jet flowed into the mock pump, a backward flow existed near the inlet port at mid-diastole (Figs. 6, detail C; 9a).

Discussion

In the present study, the flow behavior in the planes parallel and perpendicular to the circular flow (flow behavior in the PVDhJ, PIA, and POA) in our diaphragm-type blood pump was visualized and analyzed from different directions (front view, inlet, and outlet side views). Moreover, we

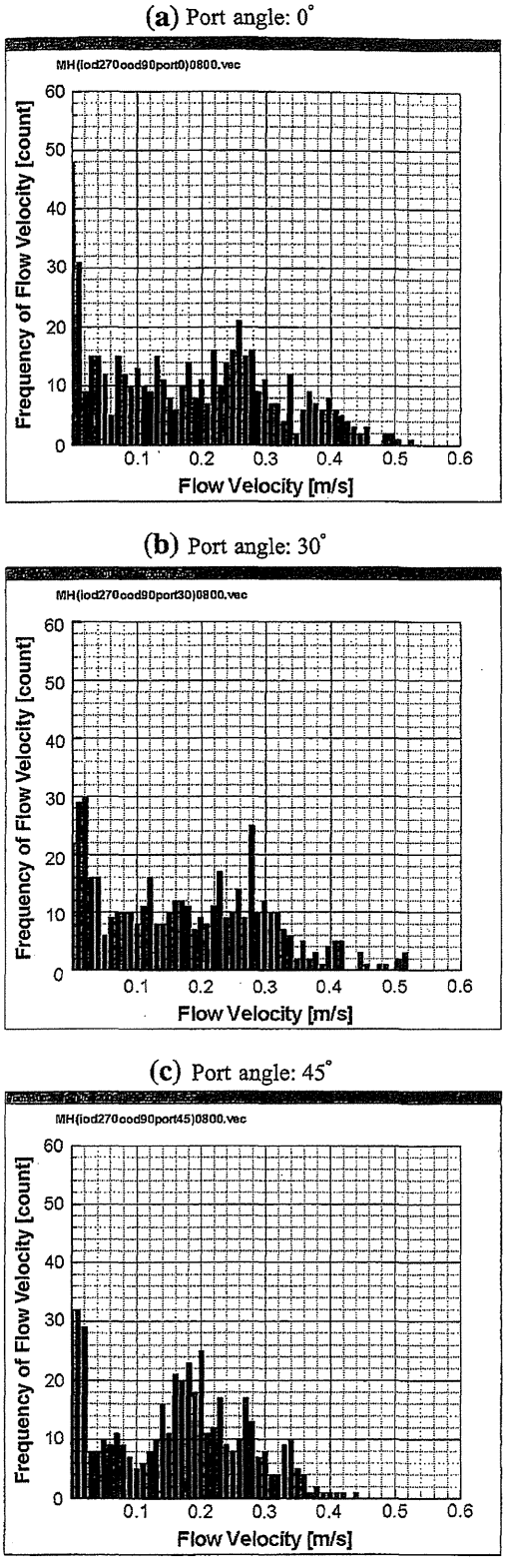

Fig. 8 Frequency distributions of the magnitude of the flow velocity vectors during end diastole. **a** Port angle of 0°, **b** port angle of 30°, **c** port angle of 45°

also evaluated the effects of the port angle, which is one of the pump configuration parameters, on the flow behavior using the PIV method.

When the port angle was 0°, the circular flow took the form of a major segment at end diastole (Fig. 5c, front view). The flow pattern of the major segment was thought to be affected by the asymmetric configuration within the housing between the inlet and outlet ports (Fig. 2b). The flow velocity downstream of the inlet valve during the diastolic phase was extremely high, and it abruptly decreased from the inlet valve to the housing inside (Fig. 5a, circle A). On the other hand, the flow velocity inside the outlet port during the systolic phase gradually increased from the housing inside to the outlet valve (Fig. 5d, circle B). This was thought to be because the configuration from the inlet port into the housing abruptly changed and radically expanded the flow field, while the configuration from within the housing to the outlet port gradually changed and moderately narrowed the flow field (Fig. 2b). With regard to the flow components in the PIA and POA, the flow patterns were almost uniform and parallel to the plane of the DhJ from end diastole to early systole (inlet side view and outlet side view of Fig. 5c, d). The main flow behavior in the mock pump was parallel to the plane of the DhJ and orderly, although the inlet jet flowed into the plane of the DhJ diagonally. The main flow inside this pump was therefore circular, and the front view was suitable for confirming the flow behavior (which was analyzed from different directions). As the laser sheets targeted the inside of the housing and illuminated the PIA or POA, the ends of the ports were not illuminated.

Nakata et al. [4] suggested that the washout effect in their blood pump depended on the flow velocity and the circular/disordered main flow pattern, based on results obtained using the laser light sheet method and the paint erosion method. In this study, it was confirmed that the flow behavior in the blood pump was affected by the port angle. When the port angles were 30° and 45°, there were circular flows that were similar to that of 0°, but the circular flow became more disorderly when the port angle increased (Fig. 6). At a port angle of 45°, the flow distortion and eccentricity of the circular flow at end diastole exceeded those for a port angle of 30°, whereas the circular flow at end diastole was slightly eccentric at a port angle of 30° (Figs. 6b–d, 7). The proportion of high flow velocity vectors (e.g., >0.4 or >0.3 m/s) during end diastole in the PVDhJ decreased as the port angle increased (Fig. 8). These results suggested that a port angle of 0° may be suitable for configuring our diaphragm-type blood pump, because it gave the greatest proportion of high flow velocity vectors, which may lead to optimal washout.

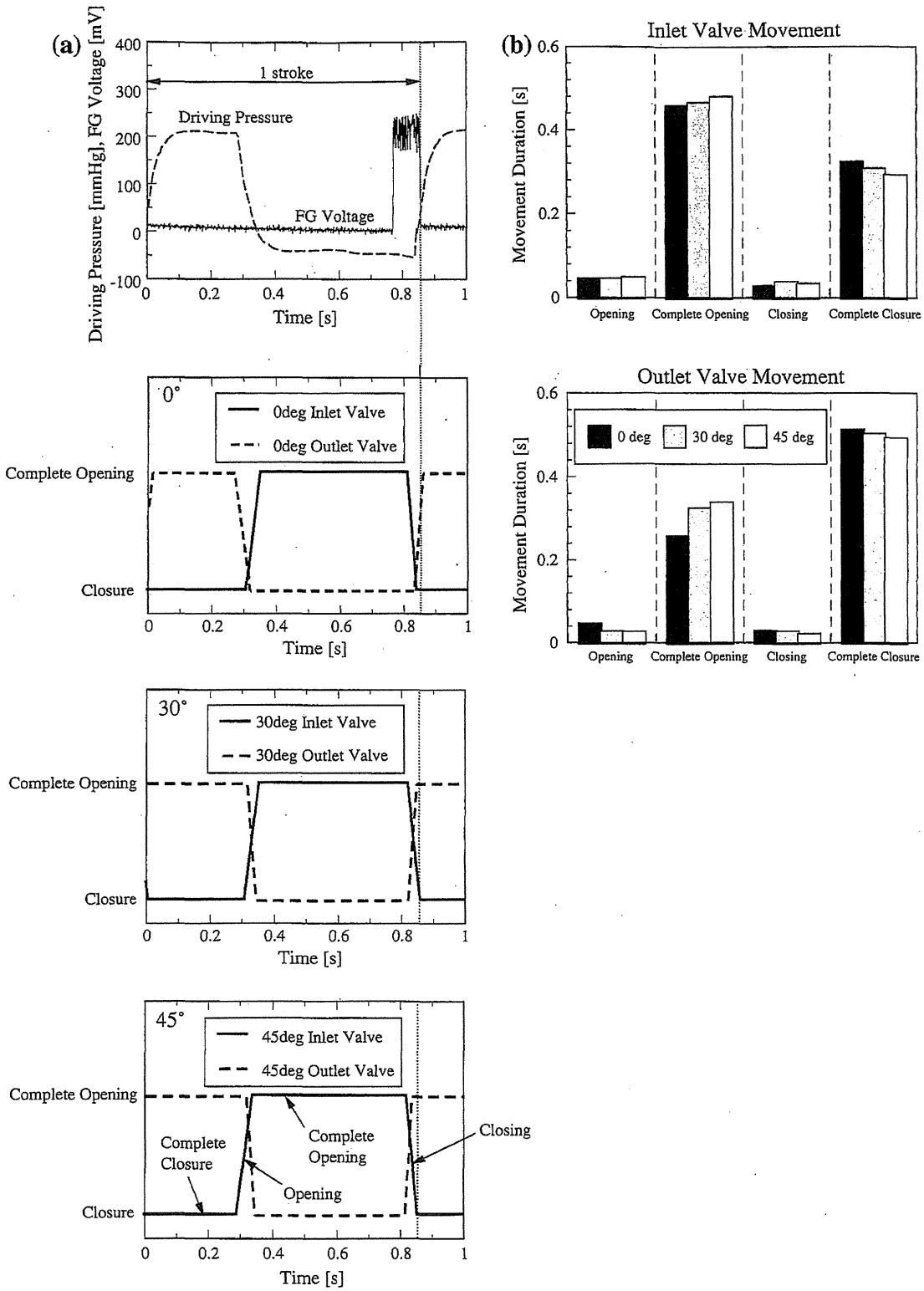

Fig. 9 Motion of the inlet and outlet valves at port angles of 0–45°. **a** Time-course changes for the opening and closing states of the inlet and outlet valves, **b** movement durations of the inlet and outlet valves

However, to confirm these washout effects, the results of chronic animal experiments will be considered.

In this study, it was confirmed that the opening and closing motions of the inlet and outlet valves were affected by the port angle. Although the outlet valve started to open after the inlet valve had almost completely closed at a port angle of 0°, the outlet valve started to open while the inlet valve was still closing at a port angle of 30° (Fig. 9a, 0° and 30°). At a port angle of 45°, the outlet valve started to open shortly after the inlet valve had started to close (Fig. 9a, 45°). The period of time that both inlet and outlet valves were completely open increased as the port angle increased (Fig. 9b). Although the drive conditions of these port angles were the same, the interval between the points at which the inlet valve started to close and the outlet valve started to open decreased with increasing port angle. Moreover, at a port angle of 45°, a backward flow was seen near the inlet port at mid-diastole to end diastole (Fig. 6, detail C, detail D). Although the inlet valve was open and the inlet jet flowed into the mock pump, a backward flow existed near the inlet port at mid-diastole (Figs. 6, detail C; 9a). The flow distortion and eccentricity of the circular flow at end diastole increased with increasing port angle, and this difference in flow behavior may have affected the propagation of the change in fluid pressure, causing this reduction in the interval between the closing and opening of the valves. However, it is not clear from this study how the difference in flow behavior affects the propagation of the change in fluid pressure, shortening the interval between the closing and opening of the valves. Further studies are necessary to confirm this mechanism, such as studies that measure the changes in the pressure distribution in the blood pump.

Because backward flow is undesirable, a port angle of 45° was considered to be unsuitable for our blood pump. Since the circular flow ran along the DhJ, it is possible that the circular flow was disturbed in the area where the stream diverged to the housing and outlet port, and the divergence subsequently affected the flow velocity and flow direction.

Conclusion

The main flow behavior inside the mock pump was a circular flow that was almost uniform and parallel to the plane of the DhJ. This circular flow became more disorderly and the proportion of high flow velocity vectors in the PVDhJ decreased as the port angle increased. These results suggest that a port angle of 0° may be suitable for our diaphragm-type blood pump when used as an extracorporeal VAD in view of the washout effect. However, the models with port angles of 30° or 45° (configurations for an implantable VAD) showed flow distortions in the present study. Therefore, further design modifications will be made in future studies.

Acknowledgments This study was partially supported by the Program for Promotion of Fundamental Studies in Health Sciences of the National Institute of Biomedical Innovation (NIBIO) and by a Grant-in-Aid for Scientific Research from the Japan Society for the Promotion of Science (JSPS).

References

1. Meier D, Wernicke JT, Orime Y, Takatani S, Tasai K, Damm G, Naito K, Mizuguchi K, Makinouchi K, Glueck J, Shimono T, Matsuda Y, Ohara Y, Kojima R, Noon GP, DeBakey ME, Nose Y. Flow pattern analysis of the Baylor total artificial heart. Artif Organs. 1994;18:923–32.
2. Watanabe N, Masuda T, Iida T, Kataoka H, Fujimoto T, Takatani S. Quantification of the secondary flow in a radial coupled centrifugal blood pump based on particle tracking velocimetry. Artif Organs. 2005;29:26–35.
3. Sakuma I, Tadokoro H, Fukui Y, Dohi T. Flow visualization study on centrifugal blood pump using a high speed video camera. Artif Organs. 1995;19:665–70.
4. Nakata M, Masuzawa T, Tatsumi E, Taenaka Y, Nishimura T, Tsukiya T, Takano H, Tsuchimoto K, Ohba K. Characterization and optimization of the flow pattern inside a diaphragm blood pump based on flow visualization techniques. ASAIO J. 1998;44: M714–8.
5. Akagawa E, Lee H, Tatsumi E, Homma A, Tsukiya T, Katagiri N, Kakuta Y, Nishinaka T, Mizuno T, Ota K, Kansaku R, Taenaka Y. Effects of mechanical valve orifice direction on the flow pattern in a ventricular assist device. J Artif Organs. 2007;10: 85–91.
6. Kreider JW, Manning KB, Oley LA, Fontaine AA, Deutsch S. The 50 cc Penn State left ventricular assist device: a parametric study of valve orientation flow dynamics. ASAIO J. 2006;52: 123–31.
7. Oley LA, Manning KB, Fontaine AA, Deutsch S. Off-design considerations of the 50 cc Penn State ventricular assist device. Artif Organs. 2005;29:378–86.
8. Mussivand T, Day KD, Naber BC. Fluid dynamic optimization of a ventricular assist device using particle image velocimetry. ASAIO J. 1999;45:25–31.
9. Hochareon P, Manning KB, Fontaine AA, Tarbell JM, Deutsch S. Correlation of in vivo clot deposition with the flow characteristics in the 50 cc Penn State artificial heart: a preliminary study. ASAIO J. 2004;50:537–42.
10. Tsukiya T, Taenaka Y, Tatsumi E, Takano H. Visualization study of the transient flow in the centrifugal blood pump impeller. ASAIO J. 2002;48:431–6.
11. Akutsu T, Saito J. Dynamic particle image velocimetry flow analysis of the flow field immediately downstream of bileaflet mechanical mitral prostheses. J Artif Organs. 2006;9:165–78.
12. Akutsu T, Saito J, Imai R, Suzuki T, Cao XD. Dynamic particle image velocimetry study of the aortic flow field of contemporary mechanical bileaflet prostheses. J Artif Organs. 2008;11:75–90.
13. Donovan FM Jr. Design of a hydraulic analog of the circulatory system for evaluating artificial hearts. Biomater Med Devices Artif Organs. 1975;3:439–49.

J Artif Organs (2012) 15:128–133
DOI 10.1007/s10047-011-0615-3

ORIGINAL ARTICLE

Alteration of LV end-diastolic volume by controlling the power of the continuous-flow LVAD, so it is synchronized with cardiac beat: development of a native heart load control system (NHLCS)

Akihide Umeki · Takashi Nishimura · Masahiko Ando · Yoshiaki Takewa · Kenji Yamazaki · Shunei Kyo · Minoru Ono · Tomonori Tsukiya · Toshihide Mizuno · Yoshiyuki Taenaka · Eisuke Tatsumi

Received: 23 June 2011 / Accepted: 26 October 2011 / Published online: 12 November 2011

Abstract There are many reports comparing pulsatile and continuous-flow left ventricular assist devices (LVAD). But continuous-flow LVAD with the pulsatile driving technique had not been tried or discussed before our group's report. We have previously developed and introduced a power-control unit for a centrifugal LVAD (EVAHEART®; Sun Medical), which can change the speed of rotation so it is synchronized with the heart beat. By use of this unit we analyzed the end-diastolic volume (EDV) to determine whether it is possible to change the native heart load. We studied 5 goats with normal hearts and 5 goats with acute LV dysfunction because of microembolization of the coronary artery. We used 4 modes, "circuit-clamp", "continuous", "counter-pulse", and "co-pulse", with the bypass rate (BR) 100%. We raised the speed of rotation of the LVAD in the diastolic phase with the counter-pulse mode, and raised it in the systolic phase with the co-pulse mode. As a result, the EDV decreased in the counter-pulse mode and increased in the co-pulse mode, compared with the continuous mode ($p < 0.05$), in both the normal and acute-heart-failure models. This result means it may be possible to achieve favorable EDV and native heart load by controlling the rotation of continuous-flow LVAD, so it is synchronized with the cardiac beat. This novel driving system may be of great benefit to patients with end-stage heart failure, especially those with ischemic etiology.

Keywords Continuous-flow LVAD · Synchronization with cardiac beat · End-diastolic volume · Heart load

A. Umeki (✉) · Y. Takewa · T. Tsukiya · T. Mizuno · Y. Taenaka · E. Tatsumi
Department of Artificial Organ,
National Cerebral and Cardiovascular Center,
5-7-1 Fujishiro-dai, Suita, Osaka 565-8565, Japan
e-mail: louvre1974@yahoo.co.jp

A. Umeki · T. Nishimura (✉) · M. Ando · S. Kyo · M. Ono
Department of Cardiothoracic Surgery, The University of Tokyo,
7-3-1 Hongo, Bunkyo-Ku, Tokyo 113-8655, Japan
e-mail: takashin-tky@umin.ac.jp

K. Yamazaki
Department of Cardiovascular Surgery, Tokyo Women's Medical University, Tokyo, Japan

Introduction

Until recently in Japan, LVAD have generally been pulsatile LVAD, but now continuous flow LVAD are being widely applied clinically, because of their long-term durability and portability. There are many reports comparing clinical outcomes and effects on circulatory dynamics after use of pulsatile and continuous-flow LVAD [1–4]. Continuous-flow LVAD with a pulsatile driving technique had not been tried or discussed before our group's report, however. Previously, we developed and introduced a power-control unit for a centrifugal LVAD (EVAHEART®; Sun Medical Technology Research Corporation, Nagano, Japan) [5, 6]. With this unit we define the distance and rotational speed (RS) of the systolic and diastolic phases to drive the EVAHEART® so it is synchronized with the native heart rate. By using normal heart goat models [7] we have already shown that we can change the coronary flow (CoF) [8] by use of its remarkable pulsatility. In the work discussed in this report we wished to determine whether it was possible to change the native heart load by use of this system, by investigating the LV end-diastolic volume (EDV) with normal and acute heart-failure models.